Strontium EXAFS Reveals the Proximity of Calcium to the Manganese Cluster of Oxygen-Evolving Photosystem II

Roehl M. Cinco,[†,‡] John H. Robblee,[†,‡] Annette Rompel,[†,‡,§] Carmen Fernandez,[‡] Vittal K. Yachandra,[*,‡] Kenneth Sauer,[*,†,‡] and Melvin P. Klein[*,‡]

Physical Biosciences Division, Lawrence Berkeley National Laboratory, and Department of Chemistry, University of California, Berkeley, California 94720-5230

Received: March 26, 1998; In Final Form: July 10, 1998

The oxygen-evolving complex of Photosystem II (PS II) in green plants and algae contains a cluster of four manganese atoms in the active site, which catalyzes the photoinduced oxidation of water to dioxygen. Along with Mn, calcium and chloride ions are necessary cofactors for proper functioning of the complex. A key unresolved question is whether Ca is close to the Mn cluster, within about 3.5 Å. To further test and verify this finding, we substituted strontium for Ca and probed from the Sr point-of-view for any nearby Mn. Sr has been shown to replace Ca and still maintain enzyme activity (about 40% of normal rate). The extended X-ray absorption fine structure (EXAFS) of Sr−PS II probes the local environment around the Sr cofactor to detect any nearby Mn. We focused on the functional Sr by removing nonessential, loosely bound Sr in the protein environment. For comparison, an inactive sample was prepared by treating the intact PS II with hydroxylamine to disrupt the Mn cluster and to produce nonfunctional enzyme. Sr EXAFS results indicate major differences in the phase and amplitude between the functional (intact) and nonfunctional (NH_2OH-treated) samples. In intact samples, the Fourier transform of the Sr EXAFS shows a peak that is missing in inactive samples. This Fourier peak II is best simulated by two Mn neighbors at a distance of 3.5 Å. Thus, with X-ray absorption studies on Sr-reconstituted PS II, we confirm the proximity of Ca (Sr) cofactor to the Mn cluster and show that the active site is a Mn−Ca heteronuclear cluster.

Introduction

Green plants, algae, and cyanobacteria supply almost all the dioxygen in the biosphere as a byproduct of photosynthesis, through the light-driven oxidation of water:

$$2H_2O \rightarrow O_2 + 4H^+ + 4e^- \quad (1)$$

This crucial reaction is catalyzed by the oxygen-evolving complex (OEC), which is located at the donor side of Photosystem II (PS II), an intrinsic thylakoid membrane protein assembly that, along with Photosystem I, helps accomplish the net reaction:

$$H_2O + CO_2 \rightarrow O_2 + \text{carbohydrates} \quad (2)$$

Comprising the OEC are four manganese atoms, along with essential cofactors Ca^{2+} and Cl^-.[1−3] Without X-ray crystallographic information about PS II (due to the lack of suitable crystals), most of the structural knowledge about the oxygen-evolving complex has resulted from biochemical, spectroscopic, and kinetic studies targeting the catalytically active site.[4−6] By these studies, the active site of the complex is known to consist of a tetranuclear manganese cluster that cycles through five intermediates S_i ($i = 0-4$), accumulating oxidizing equivalents serially until releasing dioxygen in the transition from S_4 to S_0.[7,8] In this manner, the complex couples the one-electron photooxidation of the reaction center chlorophyll P_{680} with four-electron water oxidation without generating damaging intermediates. Much has been learned about the catalytic Mn cluster, and a working model has been proposed[4,9−11] based mainly on X-ray absorption spectroscopy (XAS) and electron paramagnetic resonance (EPR) studies. Both X-ray absorption near-edge structure (XANES) and extended X-ray absorption fine structure (EXAFS) experiments have focused on the Mn atoms of the OEC to obtain oxidation states[12,13] and structural information about this active site.[14−19]

Along with manganese and chloride, Ca is an essential cofactor in oxygen evolution.[1,2,20,21] Depleting this cofactor suppresses OEC activity, which can be restored (up to 90%) by replenishing with Ca^{2+}. Partial reactivation (up to 40%) results from addition of strontium to Ca-depleted PS II membranes,[22,23] and no other metal ions (except VO^{2+}, vanadyl ion[24]) can restore activity, making this requirement highly specific for calcium.[25−27]

Although Sr^{2+} replenishes the Ca-depleted centers to a similar extent as added Ca^{2+}, the slower kinetics of the OEC turnover yields an overall lower steady-state rate[28] (40%) at saturating light intensities. Substitution of Ca with Sr also alters the EPR multiline signal (MLS) from the S_2 state, giving narrower hyperfine splitting and different intensity patterns.[23,29−31] Most researchers addressing the stoichiometry of the Ca cofactor in PS II now conclude that functional water oxidase activity requires one essential Ca^{2+}, which can be removed by low-pH/citrate or 1.2 M NaCl wash.[25,32−35] In higher plants, another

* To whom correspondence should be addressed. Telephone: (510) 486-4330. Fax: (510) 486-6059. E-mail: vkyachandra@lbl.gov or khsauer@lbl.gov or mpklein@lbl.gov.
† Department of Chemistry.
‡ Physical Biosciences Division.
§ Present address: Institut für Biochemie, Westfälische Wilhelms-Universität, Wilhelm-Klemm-Strasse 2, 48149 Münster, Germany.

S1089-5647(98)01658-7 CCC: $15.00
Published on Web 09/09/1998

more tightly bound Ca is associated with the light-harvesting complex (LHC II) and requires harsher treatments for its removal.[36−38]

There is some debate about the environment of the Ca cofactor binding site and its function. Several investigations have involved substitution of various metals into this binding site, followed by EXAFS studies on the Mn cluster. One set of experiments using EXAFS on Sr-reactivated PS II membranes was interpreted to indicate a 3.4−3.5 Å distance between the Ca (Sr) and the Mn cluster.[39] This conclusion was based on the observation of increased amplitude in the Fourier transform peak at 3.3 Å upon replacement of Ca with Sr, a heavier atom and better X-ray scatterer. This close link is also supported by FTIR spectroscopic work[40,41] that is consistent with a carboxylate bridge between Mn and Ca. Analysis of EXAFS spectra from purified PS II membrane preparations indicated a Mn−Ca interaction at slightly longer distance[42] (∼3.6−3.7 Å). Ca depletion by NaCl washing of PS II membranes removed the 16 and 23 kDa extrinsic proteins[43] and led to a reduced amplitude for this 3.6 Å feature.[19] Because of the lower X-ray scattering ability of sodium, this result was interpreted as possible Na^+ substitution for Ca^{2+} at this distance.[19]

However, another Mn EXAFS study[44] did not detect any changes in the Fourier peak at 3.3 Å when Ca was replaced with Sr^{2+} or Dy^{3+} in PS II reaction-center complexes lacking the 16 and 23 kDa extrinsic polypeptides. These authors found no evidence of an EXAFS-detectable Mn−Ca interaction at about 3.3 Å and, therefore, no Ca within the vicinity (4 Å) of the Mn cluster. Other Mn EXAFS experiments on terbium-(III)-substituted PS II, where Tb^{3+} displaced Ca^{2+} from its binding site without prior depletion, supported this alternative view.[45] Because Tb^{3+} is a competitive inhibitor of Ca^{2+} binding, the oxygen-evolving activity was suppressed in these samples but the Mn EXAFS exhibited no change from the substituting lanthanide. Tb^{3+} was not needed to fit the ∼3.4 Å distance in the Mn EXAFS spectrum, implying a Ca binding site that is at least 4 Å away from the Mn.[45] More support came from EPR-based experiments involving Mn^{2+} substitution in Ca-depleted (inactive) PS II membranes. These results indicated that the Mn^{2+}-occupied Ca binding site was outside the first coordination region of the catalytic cluster[46] (beyond 4 Å).

Given this uncertain situation and to further test whether a Ca binding site is close to the Mn cluster, we decided to embark on a different approach: to use strontium EXAFS methods to probe from the Sr cofactor point-of-view for nearby Mn within 4 Å. This is the reverse of the previously described Mn EXAFS studies that concentrated on the Mn cluster[39,44] and probed for nearby Ca or Sr neighbors. Several factors favor Sr as the better cofactor for this XAS study. First, the X-ray energies involved (16 keV for the K-edge) are more penetrating and not attenuated by air. The higher X-ray absorption cross-section and fluorescence yield of Sr also make the experiment practicable. This study then constitutes, to our knowledge, the first application of Sr EXAFS methods to biological systems. Materials science examples of Sr EXAFS techniques[47−50] are known, dealing mainly with minerals containing Sr.

Without spectroscopic handles for Sr, such as UV−vis, EPR, or Mössbauer, X-ray absorption spectroscopy (XAS) is a valuable tool[51] because XAS is element specific and sensitive when coupled with fluorescence detection.[52,53] The technique has been widely used to probe the active sites of metalloproteins[54−56] in noncrystalline samples. In particular, EXAFS gives information about the averaged local structure (within ∼4 Å) around the absorbing metal center: radial distribution of distances, identities and number of neighbors. Scatterers can be distinguished if they have a nonproximate atomic number (Z). Distances and coordination numbers can be determined with respective accuracies of 2% and 30%.[51,54,56] The Sr EXAFS-based experiment requires PS II samples with Sr substituted for Ca while maintaining oxygen-evolving activity and a stoichiometry of 1 Sr per PS II to focus on the functional cofactor binding site. Along with reactivated Sr−PS II, we can prepare an inactivated sample by treating with hydroxylamine (NH_2OH) to disrupt the Mn cluster and suppress water oxidase activity.[57−59] A comparison can then be drawn between the coordination environments of Sr in functional and inactivated PS II to derive insight into the location of the original Ca cofactor in native PS II. From these Sr substitution experiments, EXAFS provides further evidence that the Ca (Sr) cofactor is near the Mn catalytic cluster, within ∼3.5 Å. The finding indicates that the active site of oxygen evolution is a heteronuclear Ca−Mn complex.

Experimental Section

Sr^{2+}-Reactivated PS II Sample Preparation. PS II-enriched membranes were prepared by Triton X-100 (Sigma) extraction of thylakoids from spinach.[60,61] The oxygen-evolving enzyme activity ranged from 300 to 400 μmol of O_2/mg of chlorophyll (Chl)/h. These native PS II samples were stored and frozen in buffer A (0.4 M sucrose, 50 mM 2-(*N*-morpholino)ethanesulfonic acid (MES), 30 mM NaCl, 5 mM $MgCl_2$, pH 6.5) at −20 °C before use. Glassware, utensils and plasticware were acid-washed and rinsed thoroughly with deionized water, whereas the Ca-free buffers were treated with Chelex-100 resin (Bio-Rad) to remove Ca contamination. Biochemical sample handling was done in the dark with safe green light at 4 °C. Ca depletion followed the low-pH protocol of Ono and Inoue:[25] PS II membranes were quickly but thoroughly resuspended to 0.5 mg of Chl/mL in buffer B containing 10 mM citrate (pH 3.0), 0.4 M sucrose, 20 mM NaCl and incubated for 5 min while stirring. Addition of $^1/_{10}$ volume of 0.5 M morpholinopropanesulfonic acid (MOPS) (buffer C, with 0.4 M sucrose, 30 mM NaCl, pH 7.5) returned the mixture to pH 6.5.[62,63] After the mixture was stirred for 2 min, the membranes were collected by centrifugation (10 min at 40 000 g). Incidentally, this protocol retains the 16 and 23 kDa extrinsic polypeptides.[64] The resulting pellets were reconstituted with $SrCl_2$ or $CaCl_2$ (40 mM, with 25 mM MES and 30 mM NaCl at pH 6.5) by homogenizing slowly under room light for 4 min.[23,39] Sucrose was omitted from the divalent cation buffers to speed metals reconstitution, and 2.5% ethanol (v/v) was added to minimize the $g = 4.1$ EPR signal from spinach PS II preparations.[65] After centrifugation, the samples were washed with buffer F (25 mM MES, 30 mM NaCl, 2 mM $MgCl_2$, and 2.5% ethanol at pH 6.5) and pelleted again for 15 min at 40 000 g to yield Sr-reactivated and Ca-reactivated PS II.

Sr−PS II Sample Preparation by Removal of Excess Sr. To remove the weakly bound, nonessential Sr or Ca, we used the direct Chelex treatment of PS II.[35,37,66] The Sr- or Ca-reactivated samples were resuspended in sucrose-free buffer F at a concentration of 0.25 mg of Chl/mL. Two grams of Chelex-100 per 1 mg of Chl was added, and the mixture was stirred gently for 1 h. Chelex can increase the pH of the buffer,[66] so the pH was adjusted to 6.5 before mixing with PS II. After 1 h of stirring, the suspension was filtered to separate the resin from the PS II particles. Centrifugation (10 min, 40 000 g) was followed by resuspension in buffer F (with 2.5% ethanol, v/v).

One final pelleting step was done in an ultracentrifuge (Beckman) using a Ti-60 rotor (160 000 *g*, 1.5 h). The Chelex-treated pellets, designated Sr−PS II or Ca−PS II, were transferred to Mylar-backed Lucite sample holders designed to fit in EPR and XAS cryostats. These *intact* Sr− and Ca−PS II samples were dark-adapted for 1 h (at 4 °C) to poise them in the S_1 state before freezing and storage in liquid nitrogen. The *inactive* Sr−PS II was prepared by adding 30 μL of a stock solution (100 mM) of NH_2OH to the intact Sr−PS II pellet. After incubation for 20 min and without further washing or centrifugation, the NH_2OH-saturated material was transferred to Mylar-backed sample holders and frozen in liquid nitrogen. All samples were maintained at 77 K except during transfer to and from the EPR or XAS cryostats.

Oxygen-Evolution Assays. Enzyme activity for the six different types of samples (PS II, Ca-depleted, Sr/Ca-reactivated, Sr/Ca−PS II) was assayed under saturating white light using a Clark-type oxygen electrode (Yellow Springs Instruments).[18,39] The respective divalent cations (Sr or Ca, 20 mM) were added to the Sr- or Ca-containing PS II samples to achieve maximum activity, but the Ca-depleted sample received no added cations. Chlorophyll assays were done on 80% acetone extracts[67] using updated extinction coefficients.[68] Actual concentrations used for the activity assays were 10−15 μg of Chl/mL.

EPR Spectroscopy. X-band (9.2 GHz) EPR spectra were acquired on PS II samples inside XAS Lucite holders using a Varian E-109 system equipped with a standard TE102 cavity and a Heli-tran liquid helium cryostat (Air Products). Low-temperature (8 K) spectra to monitor EPR-detectable Mn^{2+} were collected on samples before and after exposure to X-rays to check that no significant sample damage had occurred. The Ca- and Sr-treated and untreated PS II samples were poised in the S_2 state by illumination for 4 min at 200 K (dry ice/ethanol bath) using a 400 W tungsten lamp (General Electric) and an aqueous $CuSO_4$ filter (5% w/v, 7 cm path). EPR data were displayed as difference (light-minus-dark) spectra. The multiline signal in the S_2 state was used to characterize the Sr- and Ca-reactivated samples and the turnover of the OEC. For Ca-depleted PS II, illumination for 2 min at 0 °C produced the characteristic split S_3' EPR signal, centered at $g = 2$ with a 164 G width.[29,69,70]

Metals Quantitation. PS II samples were first digested in boiling, concentrated ultrapure HNO_3 (Optima brand, Fisher), then diluted to 10 mL with deionized water. Elemental analysis of Mn and Sr in the ppb range was carried out at the Microanalytical Lab in the U. C. Berkeley College of Chemistry using inductively coupled plasma and atomic emission spectroscopy (ICP-AES). The amounts of PS II per sample were calculated from the chlorophyll assays, assuming 200 Chl per PS II.[34,35,71]

EXAFS Measurements. Sr K-edge EXAFS experiments resembled those previously described for Mn.[39] Absorption was equated[72] to fluorescence (F) divided by the incident flux (I_0), which was measured by a nitrogen-filled ion chamber. For energy calibration, we simultaneously measured the absorption spectrum of solid strontium acetate, whose edge peak was assigned the value 16.120 keV, near the reference value for elemental Sr (16.105 keV).[73] Spectra were collected with 3 eV steps in the preedge region (15970−16070 eV), 1 eV steps from 16070 to 16134 eV, and 0.075 Å^{-1} steps from $k = 2.0$−13.5 Å^{-1}. Five sets of data from four separately prepared intact Sr−PS II and inactive Sr−PS II samples were collected and analyzed (50 20-min scans averaged for each set).

Data Analysis. To analyze Sr EXAFS data, we followed a procedure similar to that used for Mn data.[14,39,72] The k-space data were then truncated near the zero crossings ($k = 3.6$−13.2 Å^{-1}) before the Fourier transform was applied. Fourier filtering is commonly used to simplify curve fitting of EXAFS data and works for well-separated peaks.[56,72,74,75] Here, we focused on the important long-range interactions at $R = 3$ Å. The back-transformed, Fourier-isolated data in k-space were then subjected to curve fitting, using ab initio phase and amplitude functions calculated using the program FEFF 5.05.[76,77] FEFF functions were calculated using single-scattering curved-wave theory for a simple structural model of oxygen-ligated Sr[78,79] with Mn (or other atoms, C, O, S, P, Cl) located at different distances (3.0−4.0 Å) from the central Sr.

The normalized error sum (Φ represents the quality of the fit,[80] while the ϵ^2 error accounts for the number of variable fit parameters (p) and the number of independent data points (degrees of freedom, N_{ind})[14,39,80] and is given by a reduced χ^2 statistical function. By accounting for the degrees of freedom and the justifiable number of parameters, the χ^2 value lets one distinguish whether including more parameters (p) actually improves the fit quality. Curve-fitting was done by minimizing the error sum (Φ) using a nonlinear least-squares method while varying the parameters for each shell of scatterers: R, coordination number N, σ^2, and ΔE_0. Absolute fit quality was judged through a combination of criteria: numerically by Φ, visually by how the fit follows the amplitude envelope and phase of the data, and whether resulting parameters are chemically and physically reasonable.

TABLE 1: O_2 Activity Data[a]

sample	activity (μmol of O_2/h/mg of Chl)	% vs native PS II
native PS II (control)	268 ± 14	100
Ca-reactivated PS II	221 ± 39	82
Sr-reactivated PS II	100 ± 5	37
Ca-depleted PS II	38 ± 5	14
Ca−PS II	219 ± 4	82
Sr−PS II	99 ± 4	37

[a] Oxygen-evolving activity was assayed under saturating white light, in buffer A at 25 °C. Native (untreated) PS II was regarded as the control, and its activity was taken as 100%. The other samples tested were Ca- and Sr-reactivated (with excess Ca/Sr), Ca-depleted, and Ca- and Sr−PS II (Chelex-washed). Supplementary divalent cations (20 mM) were added to achieve maximum activity: Ca^{2+} to the native PS II and Ca-treated samples and Sr^{2+} to the Sr-treated samples. Ca-depleted PS II was tested without added cations. 2,5-Dichloro-*p*-benzoquinone (DCBQ) was used as an electron acceptor at a 2 mM final concentration, from a stock solution in dimethylsulfoxide. Standard deviations for the measurements are included.

Results

Oxygen-Evolving Activity Data. Table 1 shows representative rates of oxygen evolution in the process of preparing the Sr-substituted PS II samples. The six samples considered were native PS II (untreated), Sr- and Ca-reactivated (with excess Sr/Ca), Ca-depleted, and Sr- and Ca-PS II (Chelex-treated). The O_2 activity of untreated PS II (~300 μmol O_2/h/mg of Chl) was the control (100%), so that all other values were normalized by this number. The typical percentages shown agree with the reports for Ca-depleted and substituted samples.[81] The measure of Ca-depletion was the extent of suppression of water oxidase activity. As expected, Sr substitution induced a lower steady-state rate (~40%), which served as a useful characteristic of the treatment. We have also reproduced a previous study[28] on the light-intensity dependence of oxygen evolution in Sr- and Ca-treated PS II. Under limiting light, Sr reactivates oxygen

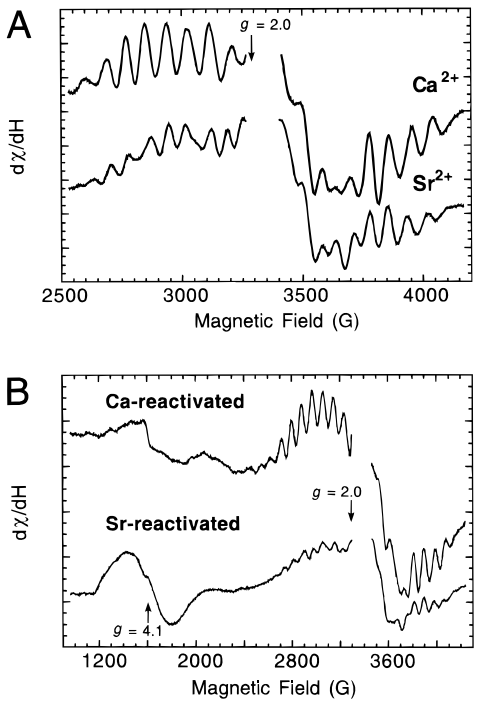

Figure 1. EPR Spectra of Sr- and Ca-reactivated PS II samples after low-pH treatment. (A) These are difference (light-minus-dark) EPR spectra of the multiline signal region for Ca- and Sr-reactivated samples. Differences are visible between the two types of samples, such as the reduced amplitude in the wings of the Sr-altered multiline signal and its different spacing compared to the Ca-reactivated MLS, which is essentially identical to that of native PS II (not shown). (B) A wider EPR scan range includes both the $g = 4$ and 2 regions. The $g = 4.1$ EPR signal is enhanced in the Sr-reactivated compared to Ca-reactivated PS II, although both samples contained 2.5% ethanol, which is reported[65] to suppress formation of this signal. For clarity, the $g = 2$ region containing the dark-stable Y^{D}_{ox} radical signal was deleted. Illumination was performed at 200 K (4 min), and all EPR spectrometer conditions were as follows: 8 K temperature, 9.21 GHz microwave frequency, 32 G modulation amplitude, 100 kHz modulation frequency, 0.5 s time constant, 30 mW microwave power, and 4 min scan time.

evolution almost as efficiently (83%) as Ca. However, during saturating light conditions, Sr reactivates only partially (40%) compared to Ca. The authors of that study concluded that Sr binding reconstitutes oxygen evolution but the rate-limiting step of the reaction is slower than for Ca.[28] For saturating light the pattern of oxygen activity is as follows: Ca-depleted 10−25%,[25,81] Sr-reactivated 30−40%,[29] Ca-reactivated 70−90%,[81] relative to control PS II (100%). The Ca−PS II and Sr−PS II values in Table 1 indicate that the Chelex wash to remove excess Sr or Ca does not harm or irreversibly inhibit the enzyme function. The data for NH_2OH-treated Sr−PS II are not shown, but the excess NH_2OH totally inhibits activity by disrupting the catalytic Mn cluster.[82]

EPR Spectroscopy. Upon substitution of Sr for Ca, an altered EPR multiline signal (MLS) appears in the difference (light-minus-dark) spectra of Sr-reactivated samples (Figure 1A). The changes were consistent with those observed previously:[23,31,39] reduced overall amplitude throughout and at the wings of the MLS, slightly narrower hyperfine splitting, and different intensity pattern. In addition, a feature at 3670 G was prominent in the Sr-reactivated compared to Ca-containing samples. A wider scan range (Figure 1B) also shows the increased amplitude of the $g = 4.1$ EPR signal in Sr-reactivated samples.[23,39,44] Together, both aspects of the light-induced (S_2) EPR signal indicated the successful replacement of Ca by Sr. After Chelex treatment, the Sr-altered MLS almost completely reverted to the normal MLS (data not shown). The causes of the loss of this diagnostic EPR signature are the subject of further investigation, but the aforementioned oxygen-evolving activity and Sr quantitation indicated the presence of functional Sr in PS II. Last, the characteristic split S_3' EPR signal was also observed in the Ca-depleted samples when illuminated at 0 °C for 2 min (data not shown). Its presence showed that Ca is removed from its cofactor binding site, with suppression of enzyme activity, before reactivation with Sr or Ca.

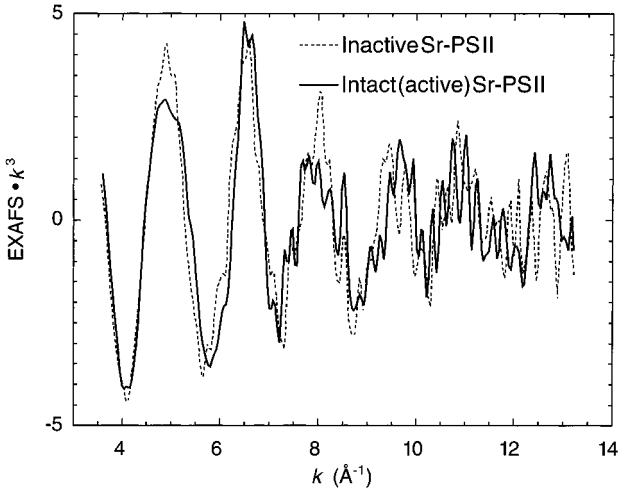

Figure 2. k^3-Weighted Sr EXAFS data of intact and inactive Sr−PS II (Chelex-treated) in the S_1 state. The average of 100 scans for each type of sample is typical of four separate data sets. The differences between the two are apparent in the amplitude envelopes and the phases, especially beyond $k \approx 9$ Å^{-1}. The intact Sr−PS II (—) has multiple frequency components, whereas the inactive, NH_2OH-treated Sr−PS II (- -) seems to possess only one component. Beyond $k \approx 12$ Å^{-1}, the inactive sample has no discernible feature in the EXAFS (only noise present).

Metals Analysis. Amounts of Sr were normalized per four Mn, the unit of functioning catalytic centers in PS II.[83,84] For Sr-reactivated samples before the Chelex treatment, Sr content was about 16 Sr per 4 Mn; this decreased to 0.75 Sr per 4 Mn upon removal of excess cation (Sr−PS II). This stoichiometry was consistent the finding that about 1 Ca^{2+} per PS II is necessary for oxygen-evolving activity.[32] Although up to 30% of Mn may be lost during the low-pH Ca-depletion step,[85] the present study focused on the Sr associated with active oxygen-evolving centers and was not so adversely affected by the Mn loss as Mn EXAFS studies would be. Because the inactive Sr−PS II samples were derived from the active samples whose Sr concentrations were determined and no washing steps were done after the hydroxylamine treatment, the Sr content within the Lucite holders for both types of (Chelex-treated) Sr−PS II samples was identical.

Sr EXAFS of Intact and Inactive Sr−PS II in the S_1 State. After the initial characterizations were completed, XAS measurements were made on the two types of (Chelex-treated) Sr−PS II: intact and inactive samples. Figure 2 shows representative unfiltered, k^3-weighted EXAFS data in k-space and illustrates the distinct differences between the two samples. The intact Sr−PS II had a reduced amplitude at $k \approx 8$ Å^{-1} resulting from the presence of more than one frequency component, whereas the inactive Sr−PS II seemed to possess only one component. The two samples also had different amplitude envelopes, beat patterns, and phases, especially beyond $k \approx 9$ Å^{-1}. The Fourier transforms of the Sr EXAFS appear in Figure 3 and reveal striking differences in the crucial $R \approx 3.0$ Å region. The noise level in both spectra was low, as shown by the

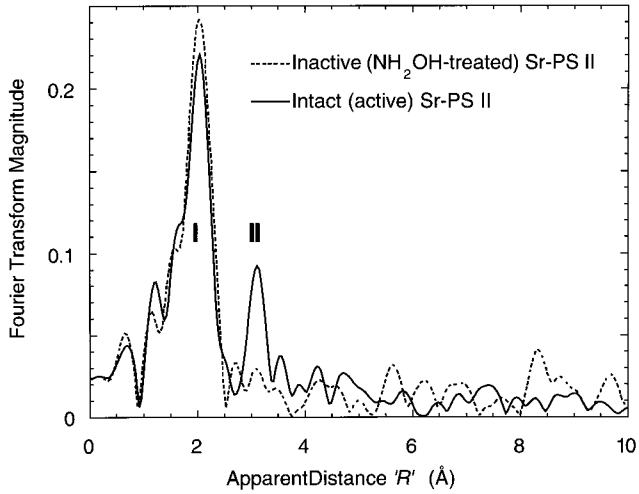

Figure 3. Fourier transforms of Sr EXAFS for intact and inactive Sr-substituted PS II samples (Chelex-treated) from Figure 2. Features around $R = 1$ Å are due to incomplete background removal. The dominant Fourier peak I is due to ligating oxygens in the first coordination sphere and is common to both samples. The two Sr−PS II samples differ mainly at the $R = 3.0$ Å region, where the intact samples exhibit Fourier peak II. This peak is present in each of the four active samples represented by this spectrum. The absence of peak II in the NH_2OH-treated sample may be a result of the disruption of the Mn cluster and serves to provide a comparison between the Sr coordination environment in the active or inactive PS II. Because it is resolved from the major peak I, peak II can be isolated for further curve fitting to determine the identity and number of contributing scatterers.

absence of major peaks beyond $R > 5$ Å. The intact Sr−PS II displayed two main Fourier peaks (I and II) at $R = 2.0$ and 3.0 Å, whereas the inactive Sr−PS II had only one major peak at $R = 2.0$ Å.

Fourier peak I dominated the spectrum for both types of Sr−PS II samples (Figure 3) and consisted of the first shell of ligating oxygens. This major feature was roughly similar in the active and inactive samples, indicating the presence of similar nearest-neighbor shells. The first peak can be simulated by 9 ± 2 oxygens at 2.57 ± 0.02 Å, where the error in coordination number is estimated at ±30%.[51] The known coordination numbers of Sr^{2+} range from 6 to 9, and Sr−O distances are distributed from 2.56 to 2.71 Å.[78,79,86] Fourier peak II ($R = 3.0$ Å) was consistently present in the four sets of intact Sr−PS II and absent in all four inactive Sr−PS II data sets. Beyond the first shell, coordination environments for Sr were different so we focus on the main point of contrast: Fourier peak II.

Curve Fitting of Sr EXAFS Data. To determine the number and identity of contributing scatterers, Fourier peak II was isolated ($\Delta R = 1.0$ Å) and back-transformed into *k*-space for curve fitting. Peak II was sufficiently resolved to allow easy separation from the dominant influence of peak I. The simulations started with chemically reasonable scatterers at about 3.5 Å from strontium, and fitting results are summarized in Table 2. First, we tried one shell of carbon at a distance of about 3.5 Å, representing light-atom scattering from possible carboxylate ligands. As Figure 4A shows, the fit was poor, especially in the middle of the range, $k \approx 6-9$ Å^{-1}, with a mismatch of amplitude envelopes and phases. The amplitude function of C, as calculated from FEFF, contains a minimum at $k \approx 7$ Å^{-1}, which probably explains the similar pattern in the carbon simulation. However, when one shell of a heavier, metal scatterer (Mn) was used, the fit improved visibly (except in the low-*k* region, 4−5 Å^{-1}) and numerically, by a factor of 3, judging from Φ. In this case, the coordination number was fixed at integer values and $N = 2$ was found to yield the best fit of the data (Figure 4B). Simulations with other low-*Z* atoms (O, P, S, Cl—Table 2) all resulted in poorer fit quality, both visibly and in Φ.

Other values for N_{Mn} were tried, such as 1 or 3, with mixed outcomes. An inadequate fit was obtained using $N = 1$ (Figure 5A), whereas $N = 3$ (Figure 5B) gave a simulation that was visually comparable to $N = 2$. Relative to $N = 2$, the

TABLE 2: Sr EXAFS Fitting Results for Peak II[a]

scatterer	R (Å)	N	σ^2 (Å^2)	ΔE_0 (eV)	$\Phi \times 10^3$	$\epsilon^2 \times 10^5$
Mn	3.55	2.0	0.0078	2.73	0.402	0.297
Mn	3.55	1.0	0.0042	1.74	1.052	0.778
Mn	3.56	3.0	0.0108	3.48	0.394	0.291
C	3.59	6.0	0.0056	2.94	1.680	1.242
O	3.56	4.0	0.0044	8.12	0.667	0.495
P	3.68	4.0	0.0082	−4.49	1.017	0.752
S	3.68	4.0	0.0089	−1.46	0.951	0.703
Cl	3.66	3.0	0.0074	−0.40	0.831	0.615

[a] Fitting parameters are as defined in the text. $S_0^2 = 0.85$ for all fits. The first four results are plotted in Figures 4A,B and 5A,B ($N_{Mn} = 2$, $N_C = 6$, $N_{Mn} = 1$, $N_{Mn} = 3$). The coordination number N was fixed to integer values for Mn and to best-fit integral values for the light atom scatterers. The goodness-of-fit values are as defined in the text. The *k*-space data range was from 3.6 to 13.2 Å^{-1}, and the Fourier filter window was 1.00 Å.

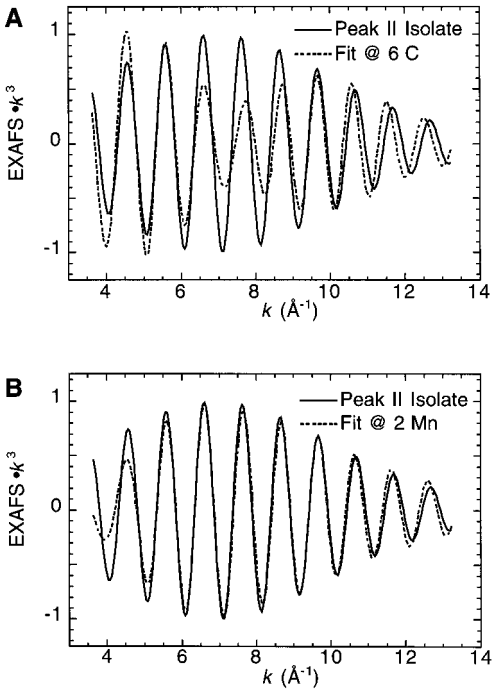

Figure 4. Sr EXAFS curve fitting for peak II with C or Mn scatterers. Simulations of peak II were done using FEFF 5.05 theoretical phases and amplitudes and minimizing the error sum (Φ) using a nonlinear least-squares method while varying these parameters for each shell of scatterers: R, σ^2, and ΔE_0. The coordination number N was then fixed at the best-fit integer value, giving a number of free parameters $p = 3$ (eq 7S). Peak II experimental data (Fourier-filtered isolate) is shown as the solid line, while the fit result is the dashed line. (**A**) When carbon (from carboxylates) was simulated as a neighbor of Sr, the fit quality was visibly poor in the middle of the *k*-range, with mismatched amplitudes and phases. (**B**) Improvement of the fit required Mn neighbors to be at a distance of ∼3.5 Å. For Mn simulations, N was fixed at integral values between 1 and 4. A coordination number of two Mn was found to best account for the data for most of the *k*-range ($k = 5-11$ Å^{-1}). Adding more shells did not significantly improve the fit quality but, instead, resulted in an underdetermined fit. Simulations using other low-*Z* atoms (O, S, P, Cl) were tried and were worse than Mn.

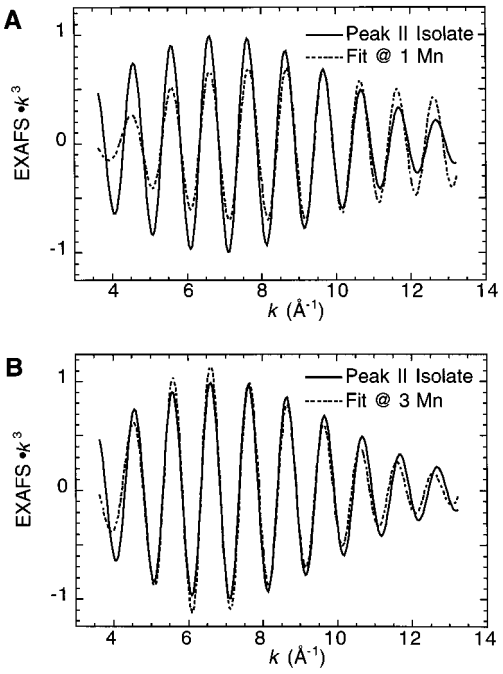

Figure 5. Sr EXAFS curve fitting for peak II with Mn scatterers. Experimental data (peak II isolate) is the solid line, and the simulation is the dashed line. (A) When N_{Mn} was fixed to 1, the fit was inadequate to describe the data throughout the *k*-range. (B) When N_{Mn} was fixed to 3, the fit improved only slightly (compared to $N_{Mn} = 2$) by exceeding the original data at the range $k = 5-7$ Å^{-1}.

improvement in fit error in going from $N = 2$ to 3 (2%) was not so dramatic as from $N = 1$ to 2 (160%). The $N = 3$ fit was accompanied by a large Debye−Waller factor (σ_2, Table 2), because *N* and σ^2 are highly correlated. Two-shell simulations have been attempted, but inclusion of another shell does not improve the fit enough to justify the increased number of free parameters (*p* in eq 7S, Supporting Information).

When peaks I and II were isolated together to minimize any possible distortions from Fourier filtering,[56] curve-fitting results (not shown) were consistent with those presented here, although dominated by first-shell scattering from peak I. Multiple scattering was neglected in this study because it was found to be insignificant unless focusing among metal atoms occurs,[74] which would be unlikely for distances as short as 3.5 Å. A theoretical EXAFS study found multiple scattering to be negligible in Photosystem II, around $R \approx 3.5$ Å.[87] The one-shell model used here was a simplified one that accounted for most of peak II. Other shells of scatterers such as C may be present, but the disordered nature of the likely ligand environments at these distances minimized their overall contribution to the EXAFS.

Discussion

The aim of this study, a novel use of EXAFS to probe Sr in biological systems, was to investigate the calcium cofactor binding site in PS II and address its proximity to the catalytic Mn cluster of the oxygen-evolving complex. To prepare samples for this study, the low-pH/citrate protocol was used to deplete Ca so that Sr could be substituted, resulting in the lower enzyme activity (40%) and the altered multiline EPR signal. Chelex treatment then removed excess, weakly bound, and adventitious Sr ions, leaving only the functioning cofactor intact, as shown by the continued oxygen activity and metals quantitation (∼1 Sr per 4 Mn). We also acquired the Mn K-edge and EXAFS spectra for one Sr−PS II sample (S_1 state, data not shown). Its K-edge spectrum resembles normal PS II in the S_1 state,[12,39] and its Fourier transform contains the customary three major peaks that are consistently observed from PS II samples.[9,14,39] Although the current study is based on Sr EXAFS, this result further ensures us that the Mn-containing centers are intact and not significantly damaged during the biochemical treatments. The biochemical and spectroscopic characterization shows that Sr has successfully replaced the original cofactor. The Sr−PS II samples, along with inactive Sr−PS II (prepared by adding NH_2OH to disrupt the intact samples), were then examined by Sr EXAFS techniques.

The Fourier transforms of the Sr EXAFS from intact Sr−PS II samples show an interaction (peak II) that is best modeled by two Mn at 3.5 Å distance. This vector is not present in the inactive, NH_2OH-treated set, although both types share similar first coordination shells of oxygen (peak I, Figure 3). Attempting to model peak II with C (the most likely low-*Z* candidate, from carboxylate ligands) results in a decidedly worse fit (Figure 4A). Other nonmetallic low-*Z* atoms (O, P, S, Cl—Table 2) also produce poor simulations compared to Mn, and so by extensive fitting trials, we have excluded light atoms as major contributors to Fourier peak II. These simulations present Mn as the chemically reasonable alternative. Strictly speaking, the EXAFS method cannot distinguish between scatterers of adjacent *Z*, so iron could also account for peak II. However, the other supporting data (biochemical studies, oxygen-evolving activity, EPR, and previous Mn EXAFS studies[39]) point to Mn as the likely candidate rather than Fe.

The coordination number for Mn that best fits the data is between 2 and 3 (Figures 4B and 5B), but for several reasons, we favor the lower number. Relative to $N = 2$, the improvement in Φ from $N = 2$ to 3 is slight (2%) compared to that from $N = 1$ to 2 (160%). Visual comparison of Figure 4B with 5B reveals that in the ranges $k \approx 5.5-7$ and $9.5-12$ Å^{-1}, $N = 2$ simulates the data more closely. Preliminary studies of the polarized Sr EXAFS from oriented Sr−PS II multilayers also show dichroism patterns that are inconsistent with $N = 3$ (R. Cinco, unpublished results).

The absence of peak II in the inactive Sr−PS II samples is consistent with the interpretation that NH_2OH disrupts the Mn cluster[58,82] and alters the Mn from its native 3.5 Å configuration. This harsh treatment may disrupt the Sr (Ca) binding site, release the cofactor, and ensure that there is no Mn nearby (within 4 Å). We believe that the NH_2OH treatment provides the best control sample for this experiment, as there is no known method to "surgically" extract the Mn cluster while leaving the cofactor unperturbed. Because no washing steps are done with the NH_2-OH-treated Sr−PS II, the Sr amount in the macroscopic sample remains identical to that of the intact Sr−PS II, and the general protein matrix is retained.

The Sr EXAFS results, translated back to the original cofactor, support the earlier conclusion that Ca (Sr) is near the Mn cluster[39] at a distance of ∼3.4−3.5 Å. Ca^{2+} has a slightly smaller radius than Sr^{2+} (by about 0.1 Å).[86] A new result from this study is that $N_{Mn} = 2$, indicating two Sr−Mn interactions, whereas the earlier Mn EXAFS study proposed one Mn−Ca (Sr) interaction. The discrepancy could ensue from the increased complexity of the Mn EXAFS signal, which is the average of contributions from the four different Mn. With each Mn having its own local environment of scatterers, especially at long distances, precise determination of *N* for the Ca (Sr) cofactor becomes difficult. Adding to the complication is the Mn−Mn interaction (at 3.3 Å)[9,17,88] that is probably also present in the same region ($R \approx 3$ Å). The conclusion based on Sr EXAFS

is more compelling because there is only one Sr per functioning catalytic center, so that its signal is neither diluted nor averaged.

For our fitting routines, we have used a simplified model involving only one shell of scatterer (Mn favored over C) to account for the long-distance interaction at 3.5 Å. This model relies on the observation that backscattering for light atoms such as C or O is probably insignificant at distances around 3.5 Å, based on EXAFS studies on complex crystalline solids.[74] There may be C scatterers present, but they are not EXAFS-detectable at these long distances because of disorder or a low backscattering amplitude. By using only one shell, we avoid an underdetermined fit where the information content of the EXAFS data does not justify the large number of adjustable parameters.

The distance of ~3.5 Å for the Sr−Mn vector indicates the presence of a single-atom bridge, likely to be oxygen.[42] This bridge may be derived from carboxylate ligands (aspartate or glutamate protein residues), protein backbone carboxyl, water, or hydroxide. This finding of a short metal−metal interaction is unprecedented for calcium-containing metalloenzymes. As discussed in an earlier study,[39] examination of calcium-binding sites in proteins and calcium complexes shows that carboxylate bridging (involving both O atoms) between two metal centers produces distances[89] of 3.8−4.3 Å, as seen in thermolysin (double Ca binding site with three bridges) and concanavalin A (Ca−Mn site with one bridge). However, in complexes where two Ca's are bridged by lone oxygen atoms from two carboxylates, shorter distances (~3.6 Å) result.[39] A polyether carboxylate complex has two single-O-atom carboxylate bridges that bring two Ca to within 3.9 Å.[90] Because Ca−O bonds are normally 2.45 Å[86] and Mn−O distances range from 1.75 to 1.9 Å,[91] replacing one Ca with a high-valent Mn (III or IV) in these bridged Ca complexes would yield a Mn−Ca distance that approaches the value found in our study (~3.5 Å). This assumes a Ca−O−Mn angle of 106°, as found in the synthesized compounds.[90] Single-O-atom bridges also help to achieve a short (3.4 Å) Sr−Ti distance in the perovskite compound $SrTiO_3$.[47] Because Ti^{4+} has a radius almost identical to that of Mn^{3+} (0.68 and 0.66 Å, respectively), if Ti were substituted with Mn, the distance would resemble the observed value from Sr EXAFS of PS II. In mixed-carboxylate/catecholate complexes that contain Mn_4LaCl and Mn_4Tb clusters, single-O-atom bridges combine to yield Mn−La and Mn−Tb distances of 3.5 and 3.2 Å, respectively.[92] The lanthanides were chosen because the ionic radii for La^{3+} (1.03 Å) and Tb^{3+} (0.92 Å) are similar to that for Ca^{2+} (1.00 Å).[86] Finally, a Mn^{III}-Schiff base complex features a manganese−sodium interaction, bridged by one acetate and O atoms from two phenolate groups.[93] With the Mn−Na distance of 3.3 Å, this complex has relevance because the ionic radius of Na^+ (1.02 Å)[94] nearly equals that of Ca^{2+}. Compared to motifs found in relevant synthesized complexes, our results are compatible with the presence of single-O-atom bridging (oxygen) between the Mn and Ca (Sr) cofactor to achieve the relatively short ~3.5 Å vector.

A model of the OEC that is topologically consistent with the new findings is presented in Figure 6, which incorporates two Mn−Ca interactions at a ~3.4−3.5 Å distance and single-O-atom bridging. For simplicity, other ligands or bridges that may be present are not depicted. This model represents one configuration, with Ca spanning the "open" end of the Mn cluster, although other modes of placing Ca between two Mn are possible (such as Ca spanning the "closed" end or extending across the top or bottom Mn pairs). Further studies to place constraints on the geometry and relative orientation of the Mn−Ca (Sr) vectors will rely on X-ray absorption linear dichroism[14,15,17,95,96] to target Fourier Peak II from the Sr EXAFS. To provide further refinement of the proposed model, polarized Sr EXAFS experiments on oriented Sr−PS II multilayers are in progress.

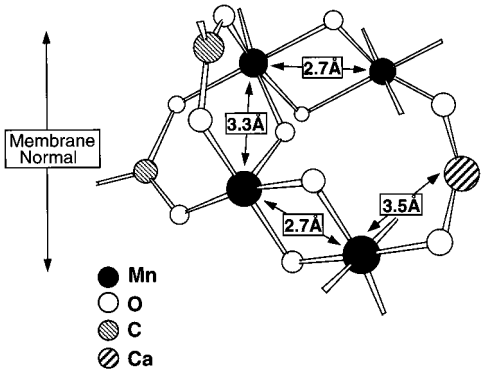

Figure 6. Proposed model for the active site of the oxygen-evolving complex (OEC) in PS II. The model incorporates the finding from the Sr-substituted PS II studies: Sr (and therefore Ca) is intimately linked to the Mn cluster at distance of ~3.4−3.5 Å. This linkage requires single-atom (oxygen) bridging that can derive from acidic protein residues (aspartate or glutamate), hydroxide, or water. Depicted is one simple configuration consistent with the findings of the Sr EXAFS study; other topologies having two Mn−Ca interactions are possible. Adapted from ref 9.

The intimate link between Ca and Mn that had been suggested in previous studies has led to the description of the catalytic center of the OEC as a "tetra-Mn/Ca cluster".[97] The present study provides concrete evidence to reinforce this concept, now that the EXAFS technique extended to strontium in biological samples has confirmed the proximity of Ca to the Mn cluster. Moreover, this approach holds promise for probing the role of the Ca cofactor in the mechanism of oxygen evolution.

Acknowledgment. This research was supported by the Director, Office of Basic Energy Sciences, Division of Energy Biosciences of the U.S. Department of Energy (DOE), under Contract No. DE-AC03-76SF00098, and the National Institutes of Health (GM55302 to V.K.Y.). Synchrotron radiation facilities were provided by the Stanford Synchrotron Radiation Laboratory (SSRL) which is operated by the Department of Energy, Office of Basic Energy Sciences. The SSRL Biotechnology Program is supported by the National Institutes of Health, National Center of Research Resources, Biomedical Technology Program, and by the Department of Energy, Office of Health and Environmental Research. R.M.C. is grateful to the Ford Foundation for a predoctoral fellowship. Additional financial support was also provided by the Fundacao de Amparo a Pesquisa do Estado de Sao Paulo (to C.F.), and the Deutsche Forschungsgemeinschaft (to A.R.). Prof. Hubert Schmidbaur and Michael Schmidt kindly provided the Sr−amino-acid complexes mentioned. We also thank Dr. Matthew Latimer, Dr. Wa On Yu, and Joanne Miura for help with the data collection and sample preparation.

Supporting Information Available: Supporting Information Available: Expanded Experimental Section with further details on EXAFS data acquisition and analysis (3 pages). See any current masthead page for ordering and Internet access instructions.

References and Notes

(1) Debus, R. J. *Biochim. Biophys. Acta* **1992**, *1102*, 269−352.
(2) Yocum, C. F. *Biochim. Biophys. Acta* **1991**, *1059*, 1−15.

(3) Homann, P. H. *Biochim. Biophys. Acta* **1988**, *934*, 1−13.
(4) Yachandra, V. K.; Sauer, K.; Klein, M. P. *Chem. Rev.* **1996**, *96*, 2927−2950.
(5) Britt, R. D. In *Oxygenic Photosynthesis: The Light Reactions*; Ort, D. R., Yocum, C. F., Eds.; Kluwer Academic Publishers: Dordrecht, 1996; pp 137−164.
(6) Renger, G. *Physiol. Plant.* **1997**, *100*, 828−841.
(7) Kok, B.; Forbush, B.; McGloin, M. *Photochem. Photobiol.* **1970**, *11*, 457−476.
(8) Joliot, P.; Kok, B. In *Bioenergetics of Photosynthesis*; Govindjee, Ed.; Academic Press: New York, 1975; pp 387−412.
(9) Yachandra, V. K.; DeRose, V. J.; Latimer, M. J.; Mukerji, I.; Sauer, K.; Klein, M. P. *Science* **1993**, *260*, 675−679.
(10) Wieghardt, K. *Angew. Chem., Int. Ed. Engl.* **1994**, *33*, 725−728.
(11) Sauer, K.; Yachandra, V. K.; Britt, R. D.; Klein, M. P. In *Manganese Redox Enzymes*; Pecoraro, V. L., Ed.; VCH Publishers: New York, 1992; pp 141−175.
(12) Roelofs, T. A.; Liang, W.; Latimer, M. J.; Cinco, R. M.; Rompel, A.; Andrews, J. C.; Sauer, K.; Yachandra, V. K.; Klein, M. P. *Proc. Natl. Acad. Sci. U.S.A.* **1996**, *93*, 3335−3340.
(13) Ono, T.-A.; Noguchi, T.; Inoue, Y.; Kusunoki, M.; Matsushita, T.; Oyanagi, H. *Science* **1992**, *258*, 1335−1337.
(14) Dau, H.; Andrews, J. C.; Roelofs, T. A.; Latimer, M. J.; Liang, W.; Yachandra, V. K.; Sauer, K.; Klein, M. P. *Biochemistry* **1995**, *34*, 5274−5287.
(15) Mukerji, I.; Andrews, J. C.; DeRose, V. J.; Latimer, M. J.; Yachandra, V. K.; Sauer, K.; Klein, M. P. *Biochemistry* **1994**, *33*, 9712−9721.
(16) Riggs, P. J.; Mei, R.; Yocum, C. F.; Penner-Hahn, J. E. *J. Am. Chem. Soc.* **1992**, *114*, 10650−10651.
(17) George, G. N.; Prince, R. C.; Cramer, S. P. *Science* **1989**, *243*, 789−791.
(18) DeRose, V. J.; Mukerji, I.; Latimer, M. J.; Yachandra, V. K.; Sauer, K.; Klein, M. P. *J. Am. Chem. Soc.* **1994**, *116*, 5239−5249.
(19) MacLachlan, D. J.; Nugent, J. H. A.; Bratt, P. J.; Evans, M. C. W. *Biochim. Biophys. Acta* **1994**, *1186*, 186−200.
(20) Boussac, A.; Rutherford, A. W. *Biochem. Soc. Trans.* **1994**, *22*, 352−358.
(21) Boussac, A.; Rutherford, A. W. *Photosynth. Res.* **1992**, *32*, 207−209.
(22) Ghanotakis, D. F.; Babcock, G. T.; Yocum, C. F. *FEBS Lett.* **1984**, *167*, 127−130.
(23) Boussac, A.; Rutherford, A. W. *Biochemistry* **1988**, *27*, 3476−3483.
(24) Lockett, C. J.; Demetriou, C.; Bowden, S. J.; Nugent, J. H. A. *Biochim. Biophys. Acta* **1990**, *1016*, 213-218.
(25) Ono, T.; Inoue, Y. *FEBS Lett.* **1988**, *227*, 147−152.
(26) Ghanotakis, D. F.; Babcock, G. T.; Yocum, C. F. *Biochim. Biophys. Acta* **1985**, *809*, 173−180.
(27) Ono, T.-A.; Inoue, Y. *Arch. Biochem. Biophys.* **1989**, *275*, 440−448.
(28) Boussac, A.; Rutherford, A. W. *Chem. Script.* **1988**, *28A*, 123−126.
(29) Boussac, A.; Zimmermann, J.-L.; Rutherford, A. W. *Biochemistry* **1989**, *28*, 8984−8989.
(30) Sivaraja, M.; Tso, J.; Dismukes, G. C. *Biochemistry* **1989**, *28*, 9459−9464.
(31) Tso, J.; Sivaraja, M.; Dismukes, G. C. *Biochemistry* **1991**, *30*, 4734−4739.
(32) Ädelroth, P.; Lindberg, K.; Andréasson, L.-E. *Biochemistry* **1995**, *34*, 9021−9027.
(33) Cammarata, K. V.; Cheniae, G. M. *Plant Physiol.* **1987**, *84*, 587−595.
(34) Shen, J.-R.; Satoh, K.; Katoh, S. *Biochim. Biophys. Acta* **1988**, *933*, 358−364.
(35) Katoh, S.; Satoh, K.; Ohno, T.; Chen, J.-R.; Kashino, Y. In *Progress in Photosynthesis Research*; Biggins, J., Ed.; Martinus Nijhoff Publishers: Dordrecht, 1987; Vol. I, pp I.5.625−628.
(36) Davis, D. J.; Gross, E. L. *Biochim. Biophys. Acta* **1975**, *387*, 557−567.
(37) Han, K.-C.; Katoh, S. *Plant Cell Physiol.* **1993**, *34*, 585−593.
(38) Chen, C.; Kazimir, J.; Cheniae, G. M. *Biochemistry* **1995**, *34*, 13511−13526.
(39) Latimer, M. J.; DeRose, V. J.; Mukerji, I.; Yachandra, V. K.; Sauer, K.; Klein, M. P. *Biochemistry* **1995**, *34*, 10898−10909.
(40) Noguchi, T.; Ono, T.-A.; Inoue, Y. In *Photosynthesis: from Light to Biosphere*; Mathis, P., Ed.; Kluwer Academic Publishers: Dordrecht, The Netherlands, 1995; Vol. II, pp 235−240.
(41) Noguchi, T.; Ono, T.-A.; Inoue, Y. *Biochim. Biophys. Acta* **1995**, *1228*, 189−200.
(42) MacLachlan, D. J.; Hallahan, B. J.; Ruffle, S. V.; Nugent, J. H. A.; Evans, M. C. W.; Strange, R. W.; Hasnain, S. S. *Biochem. J.* **1992**, *285*, 569−576.
(43) Seidler, A. *Biochim. Biophys. Acta* **1996**, *1277*, 35−60.
(44) Riggs-Gelasco, P. J.; Mei, R.; Ghanotakis, D. F.; Yocum, C. F.; Penner-Hahn, J. E. *J. Am. Chem. Soc.* **1996**, *118*, 2400−2410.
(45) Hatch, C.; Grush, M.; Bradley, R.; LoBrutto, R.; Cramer, S.; Frasch, W. In *Photosynthesis: from Light to Biosphere*; Mathis, P., Ed.; Kluwer Academic Publishers: Dordrecht, The Netherlands, 1995; Vol. II, pp 425−429.
(46) Booth, P. J.; Rutherford, A. W.; Boussac, A. *Biochim. Biophys. Acta* **1996**, *1277*, 127−134.
(47) Fischer, M.; Bonello, B.; Itié, J. P.; Polian, A.; Dartyge, E.; Fontaine, A.; Tolentino, H. *Phys. Rev. B* **1990**, *42*, 8494−8498.
(48) Kohn, S. C.; Charnock, J. M.; Henderson, C. M. B.; Greaves, G. N. *Contrib. Mineral. Petrol.* **1990**, *105*, 359−368.
(49) Papelis, C.; Chen, C.-C.; Hayes, K. F. In *SSRL 1995 Activity Report*; Cantwell, K., Dunn, L., Eds.; Stanford Synchrotron Radiation Laboratory: Stanford, 1996; pp 206−209.
(50) Hayes, K. F.; Traina, S. J.; Papelis, C.; Katz, L. E. In *SSRL 1996 Activity Report*; Dunn, L., Ed.; Stanford Synchrotron Radiation Laboratory: Stanford, 1997; pp A-322−329.
(51) Bertagnolli, H.; Ertel, T. S. *Angew. Chem., Int. Ed. Engl.* **1994**, *33*, 45−66.
(52) Yachandra, V. K. *Methods Enzymol.* **1995**, *246*, 638−675.
(53) Jaklevic, J.; Kirby, J. A.; Klein, M. P.; Robertson, A. S.; Brown, G.; Eisenberger, P. *Solid State Commun.* **1977**, *23*, 679−682.
(54) Cramer, S. P. In *X-ray Absorption: Principles, Applications and Techniques of EXAFS, SEXAFS, and XANES*; Koningsberger, D. C., Prins, R., Eds.; Wiley-Interscience: New York, 1988; pp 257−320.
(55) Yachandra, V. K.; Klein, M. P. In *Biophysical Techniques in Photosynthesis*; Amesz, J., Hoff, A. J., Eds.; Kluwer Academic Publishers: Dordrecht, Netherlands, 1996; Vol. 3, pp 337−354.
(56) Riggs-Gelasco, P. J.; Stemmler, T. L.; Penner-Hahn, J. E. *Coord. Chem. Rev.* **1995**, *144*, 245−286.
(57) Tamura, N.; Cheniae, G. *Biochim. Biophys. Acta* **1985**, *809*, 245−259.
(58) Miller, A.-F.; Brudvig, G. W. *Biochemistry* **1989**, *28*, 8181−8190.
(59) Miyao, M.; Inoue, Y. *Biochim. Biophys. Acta* **1991**, *1056*, 47−56.
(60) Berthold, D. A.; Babcock, G. T.; Yocum, C. F. *FEBS Lett.* **1981**, *134*, 231−234.
(61) Dunahay, T. G.; Staehelin, L. A.; Seibert, M.; Ogilvie, P. D.; Berg, S. P. *Biochim. Biophys. Acta* **1984**, *764*, 179−193.
(62) Ono, T.-A.; Izawa, S.; Inoue, Y. *Biochemistry* **1992**, *31*, 7648−7655.
(63) Kodera, Y.; Hara, H.; Astashkin, A. V.; Kawamori, A.; Ono, T.-A. *Biochim. Biophys. Acta* **1995**, *1232*, 43−51.
(64) Shen, J.-R.; Katoh, S. *Plant Cell Physiol.* **1991**, *32*, 439−446.
(65) Zimmermann, J.-L.; Rutherford, A. W. *Biochemistry* **1986**, *25*, 4609−4615.
(66) Kashino, Y.; Satoh, K.; Katoh, S. *FEBS Lett.* **1986**, *205*, 150−154.
(67) Arnon, D. I. *Plant Physiol.* **1949**, *24*, 1−15.
(68) Porra, R. J.; Thompson, W. A.; Kriedemann, P. E. *Biochim. Biophys. Acta* **1989**, *975*, 384−394.
(69) Boussac, A.; Zimmermann, J.-L.; Rutherford, A. W. *FEBS Lett.* **1990**, *227*, 69−74.
(70) Astashkin, A. V.; Mino, H.; Kawamori, A.; Ono, T.-A. *Chem. Phys. Lett.* **1997**, *272*, 506−516.
(71) Grove, G. N.; Brudvig, G. W. *Biochemistry* **1998**, *37*, 1532−1539.
(72) Teo, B. K. *EXAFS: Basic Principles and Data Analysis*; Springer-Verlag: Berlin, 1986.
(73) *Center for X-ray Optics X-ray Data Booklet*; Vaughan, D., Ed.; Lawrence Berkeley Laboratory: Berkeley, CA, 1986; PUB-490 Rev.
(74) O'Day, P. A.; Rehr, J. J.; Zabinsky, S. I.; Brown, G. E., Jr. *J. Am. Chem. Soc.* **1994**, *116*, 2938−2949.
(75) Lin, S.-L.; Stern, E. A.; Kalb (Gilboa), A. J.; Zhang, Y. *Biochemistry* **1991**, *30*, 2323−2332.
(76) Rehr, J. J.; Mustre de Leon, J.; Zabinsky, S. I.; Albers, R. C. *J. Am. Chem. Soc.* **1991**, *113*, 5135−5140.
(77) Rehr, J. J.; Albers, R. C.; Zabinsky, S. I. *Phys. Rev. Lett.* **1992**, *69*, 3397−3400.
(78) Schmidbaur, H.; Bach, I.; Wilkinson, D. L.; Müller, G. *Chem. Ber.* **1989**, *122*, 1433−1438.
(79) Schmidbaur, H.; Mikulcik, P.; Müller, G. *Chem. Ber.* **1990**, *123*, 1599−1602.
(80) Binsted, N.; Strange, R. W.; Hasnain, S. S. *Biochemistry* **1992**, *31*, 12117−12125.
(81) Ono, T.; Inoue, Y. *Biochim. Biophys. Acta* **1989**, *973*, 443−449.
(82) Miller, A.-F.; Brudvig, G. W. *Biochemistry* **1990**, *29*, 1385−1392.
(83) Ananyev, G. M.; Dismukes, G. C. *Biochemistry* **1996**, *35*, 4102−4109.
(84) Ohno, T.-A.; Satoh, K.; Katoh, S. *Biochim. Biophys. Acta* **1986**, *852*, 1−8.
(85) Shen, J.-R.; Inoue, Y. *Plant Cell Physiol.* **1991**, *32*, 453−457.

(86) Rees, W. S., Jr. In *Encyclopedia of Inorganic Chemistry*; King, R. B., Ed.; John Wiley & Sons: Chichester, 1994; Vol. 1, pp 67−87.
(87) Dittmer, J.; Dau, H. *Ber. Bunsen-Ges. Phys. Chem.* **1996**, *100*, 1993−1998.
(88) Riggs-Gelasco, P. J.; Mei, R.; Yocum, C. F.; Penner-Hahn, J. E. *J. Am. Chem. Soc.* **1996**, *118*, 2387−2399.
(89) Kretsinger, R. H.; Nelson, D. J. *Coord. Chem. Rev.* **1976**, *18*, 29−124.
(90) Bahl, A. M.; Krishnaswamy, S.; Massand, N. G.; Burkey, D. J.; Hanusa, T. P. *Inorg. Chem.* **1997**, *36*, 5413−5415.
(91) Pecoraro, V. L. In *Manganese Redox Enzymes*; Pecoraro, V. L., Ed.; VCH Publishers: New York, 1992; pp 197−231.
(92) Reynolds, R. A., III; Coucouvanis, D. *J. Am. Chem. Soc.* **1998**, *120*, 209−210.
(93) Bonadies, J. A.; Kirk, M. L.; Lah, M. S.; Kessissoglou, D. P.; Hatfield, W. E.; Pecoraro, V. L. *Inorg. Chem.* **1989**, *28*, 2037−2044.
(94) Mair, F. S.; Snaith, R. In *Encyclopedia of Inorganic Chemistry*; King, R. B., Ed.; John Wiley & Sons: Chichester, 1994; Vol. 1, pp 35−54.
(95) George, G. N.; Cramer, S. P.; Frey, T. G.; Prince, R. C. *Biochim. Biophys. Acta* **1993**, *1142*, 240−252.
(96) George, G. N.; Prince, R. C.; Frey, T. G.; Cramer, S. P. *Physica B* **1989**, *158*, 81−83.
(97) Ananyev, G. M.; Dismukes, G. C. *Biochemistry* **1997**, *36*, 11342−11350.